

Study of the Suppressed Decays $B^- \rightarrow [K^+\pi^-]_D K^-$ and $B^- \rightarrow [K^+\pi^-]_D \pi^-$

M. Saigo,⁴¹ K. Abe,⁷ K. Abe,⁴⁰ H. Aihara,⁴² M. Akatsu,²⁰ Y. Asano,⁴⁶ V. Aulchenko,¹ T. Aushev,¹¹ S. Bahinipati,⁴ A. M. Bakich,³⁷ Y. Ban,³¹ S. Banerjee,³⁸ I. Bedny,¹ U. Bitenc,¹² I. Bizjak,¹² S. Blyth,²⁴ A. Bondar,¹ A. Bozek,²⁵ M. Bračko,^{7,18,12} J. Brodzicka,²⁵ T. E. Browder,⁶ Y. Chao,²⁴ A. Chen,²² K.-F. Chen,²⁴ W. T. Chen,²² B. G. Cheon,³ R. Chistov,¹¹ S.-K. Choi,⁵ Y. Choi,³⁶ Y. K. Choi,³⁶ A. Chuvikov,³² S. Cole,³⁷ J. Dalseno,¹⁹ M. Danilov,¹¹ M. Dash,⁴⁷ L. Y. Dong,⁹ A. Drutskoy,⁴ S. Eidelman,¹ V. Eiges,¹¹ Y. Enari,²⁰ S. Fratina,¹² N. Gabyshev,¹ A. Garmash,³² T. Gershon,⁷ G. Gokhroo,³⁸ B. Golob,^{17,12} J. Haba,⁷ K. Hayasaka,²⁰ H. Hayashii,²¹ M. Hazumi,⁷ T. Higuchi,⁷ L. Hinz,¹⁶ T. Hokuue,²⁰ Y. Hoshi,⁴⁰ S. Hou,²² W.-S. Hou,²⁴ Y. B. Hsiung,²⁴ T. Iijima,²⁰ A. Imoto,²¹ K. Inami,²⁰ A. Ishikawa,⁷ R. Itoh,⁷ M. Iwasaki,⁴² Y. Iwasaki,⁷ J. H. Kang,⁴⁸ J. S. Kang,¹⁴ P. Kapusta,²⁵ N. Katayama,⁷ H. Kawai,² T. Kawasaki,²⁷ N. Kent,⁶ H. R. Khan,⁴³ H. Kichimi,⁷ H. J. Kim,¹⁵ S. K. Kim,³⁵ S. M. Kim,³⁶ K. Kinoshita,⁴ P. Koppenburg,⁷ S. Korpar,^{18,12} P. Križan,^{17,12} P. Krokovny,¹ R. Kulasiri,⁴ C. C. Kuo,²² A. Kuzmin,¹ Y.-J. Kwon,⁴⁸ G. Leder,¹⁰ S. E. Lee,³⁵ T. Lesiak,²⁵ J. Li,³⁴ S.-W. Lin,²⁴ D. Liventsev,¹¹ J. MacNaughton,¹⁰ G. Majumder,³⁸ F. Mandl,¹⁰ D. Marlow,³² T. Matsumoto,⁴⁴ A. Matyja,²⁵ Y. Mikami,⁴¹ W. Mitaroff,¹⁰ H. Miyake,²⁹ R. Mizuk,¹¹ D. Mohapatra,⁴⁷ T. Mori,⁴³ Y. Nagasaka,⁸ E. Nakano,²⁸ M. Nakao,⁷ Z. Natkaniec,²⁵ S. Nishida,⁷ O. Nitoh,⁴⁵ S. Ogawa,³⁹ T. Ohshima,²⁰ T. Okabe,²⁰ S. Okuno,¹³ S. L. Olsen,⁶ W. Ostrowicz,²⁵ H. Ozaki,⁷ P. Pakhlov,¹¹ H. Palka,²⁵ H. Park,¹⁵ K. S. Park,³⁶ N. Parslow,³⁷ L. S. Peak,³⁷ R. Pestotnik,¹² L. E. Piilonen,⁴⁷ A. Poluektov,¹ F. J. Ronga,⁷ H. Sagawa,⁷ Y. Sakai,⁷ N. Sato,²⁰ T. Schietinger,¹⁶ O. Schneider,¹⁶ P. Schönmeier,⁴¹ J. Schümann,²⁴ A. J. Schwartz,⁴ S. Semenov,¹¹ R. Seuster,⁶ M. E. Sevier,¹⁹ H. Shibuya,³⁹ J. B. Singh,³⁰ A. Somov,⁴ N. Soni,³⁰ R. Stamen,⁷ S. Stanič,^{46,*} M. Starič,¹² T. Sumiyoshi,⁴⁴ S. Suzuki,³³ S. Y. Suzuki,⁷ O. Tajima,⁷ F. Takasaki,⁷ K. Tamai,⁷ N. Tamura,²⁷ M. Tanaka,⁷ Y. Teramoto,²⁸ X. C. Tian,³¹ K. Trabelsi,⁶ T. Tsukamoto,⁷ S. Uehara,⁷ T. Uglov,¹¹ S. Uno,⁷ Y. Ushiroda,⁷ G. Varner,⁶ K. E. Varvell,³⁷ S. Villa,¹⁶ C. C. Wang,²⁴ C. H. Wang,²³ M.-Z. Wang,²⁴ M. Watanabe,²⁷ Y. Watanabe,⁴³ A. Yamaguchi,⁴¹ H. Yamamoto,⁴¹ Y. Yamashita,²⁶ M. Yamauchi,⁷ Y. Yusa,⁴¹ L. M. Zhang,³⁴ Z. P. Zhang,³⁴ V. Zhilich,¹ D. Žontar,^{17,12} and D. Zürcher¹⁶

(The Belle Collaboration)

¹*Budker Institute of Nuclear Physics, Novosibirsk*

²*Chiba University, Chiba*

³*Chonnam National University, Kwangju*

⁴*University of Cincinnati, Cincinnati, Ohio 45221*

⁵*Gyeongsang National University, Chinju*

⁶*University of Hawaii, Honolulu, Hawaii 96822*

⁷*High Energy Accelerator Research Organization (KEK), Tsukuba*

⁸*Hiroshima Institute of Technology, Hiroshima*

⁹*Institute of High Energy Physics, Chinese Academy of Sciences, Beijing*

¹⁰*Institute of High Energy Physics, Vienna*

¹¹*Institute for Theoretical and Experimental Physics, Moscow*

¹²*J. Stefan Institute, Ljubljana*

¹³*Kanagawa University, Yokohama*

¹⁴*Korea University, Seoul*

¹⁵*Kyungpook National University, Taegu*

¹⁶*Swiss Federal Institute of Technology of Lausanne, EPFL, Lausanne*

¹⁷*University of Ljubljana, Ljubljana*

¹⁸*University of Maribor, Maribor*

¹⁹*University of Melbourne, Victoria*

²⁰*Nagoya University, Nagoya*

²¹*Nara Women's University, Nara*

²²*National Central University, Chung-li*

²³*National United University, Miao Li*

²⁴*Department of Physics, National Taiwan University, Taipei*

²⁵*H. Niewodniczanski Institute of Nuclear Physics, Krakow*

²⁶*Nihon Dental College, Niigata*

²⁷*Niigata University, Niigata*

²⁸*Osaka City University, Osaka*

²⁹*Osaka University, Osaka*

³⁰Panjab University, Chandigarh

³¹Peking University, Beijing

³²Princeton University, Princeton, New Jersey 08545

³³Saga University, Saga

³⁴University of Science and Technology of China, Hefei

³⁵Seoul National University, Seoul

³⁶Sungkyunkwan University, Suwon

³⁷University of Sydney, Sydney NSW

³⁸Tata Institute of Fundamental Research, Bombay

³⁹Toho University, Funabashi

⁴⁰Tohoku Gakuin University, Tagajo

⁴¹Tohoku University, Sendai

⁴²Department of Physics, University of Tokyo, Tokyo

⁴³Tokyo Institute of Technology, Tokyo

⁴⁴Tokyo Metropolitan University, Tokyo

⁴⁵Tokyo University of Agriculture and Technology, Tokyo

⁴⁶University of Tsukuba, Tsukuba

⁴⁷Virginia Polytechnic Institute and State University, Blacksburg, Virginia 24061

⁴⁸Yonsei University, Seoul

(Dated: August 23, 2019)

We report a study of the suppressed decays $B^- \rightarrow [K^+\pi^-]_D K^-$ and $B^- \rightarrow [K^+\pi^-]_D \pi^-$, where $[K^+\pi^-]_D$ indicates that the $K^+\pi^-$ pair originates from a neutral D meson. These decay modes are sensitive to the Unitarity Triangle angle ϕ_3 . We use a data sample containing 275 million $B\bar{B}$ pairs recorded at the $\Upsilon(4S)$ resonance with the Belle detector at the KEKB asymmetric e^+e^- storage ring. The signal for $B^- \rightarrow [K^+\pi^-]_D K^-$ is not statistically significant, and we set a limit $r_B < 0.27$ at 90% confidence level, where r_B is the magnitude of the ratio of amplitudes $|A(B^- \rightarrow \bar{D}^0 K^-)/A(B^- \rightarrow D^0 K^-)|$. We observe a signal with 6.4σ statistical significance in the related mode, $B^- \rightarrow [K^+\pi^-]_D \pi^-$.

PACS numbers: 11.30.Er, 12.15.Hh, 13.25.Hw, 14.40.Nd

Precise measurements of the elements of the Cabibbo-Kobayashi-Maskawa matrix [1] constrain the standard model and may reveal new physics. However, the extraction of the Unitarity Triangle angle ϕ_3 is a challenging measurement even with modern high luminosity B factories. Several methods for measuring ϕ_3 use the interference between $B^- \rightarrow D^0 K^-$ and $B^- \rightarrow \bar{D}^0 K^-$, which occurs when D^0 and \bar{D}^0 decay to common final states [2, 3]. As noted by Atwood, Dunietz and Soni (ADS) [4], CP violation effects are enhanced if the final state is chosen so that the interfering amplitudes have comparable magnitudes; the archetype uses $B^- \rightarrow [K^+\pi^-]_D K^-$, where $[K^+\pi^-]_D$ indicates that the $K^+\pi^-$ pair originates from a neutral D meson. In this case, the color-allowed B decay followed by the doubly Cabibbo-suppressed D decay interferes with the color-suppressed B decay followed by the Cabibbo-allowed D decay (Fig. 1). Previous studies of this decay mode have not found any signals [5]. For the suppressed decay $B^- \rightarrow [K^+\pi^-]_D \pi^-$, both topology and phenomenology are similar to $B^- \rightarrow [K^+\pi^-]_D K^-$.

In this analysis, the favored decays $B^- \rightarrow [K^-\pi^+]_D h^-$, where $h = \pi$ or K , are used as control samples to reduce systematic uncertainties. The same selection criteria for the suppressed decay modes are applied to the control samples whenever possible. Throughout this report, charge conjugate states are implied except where explicitly mentioned and we denote the analyzed

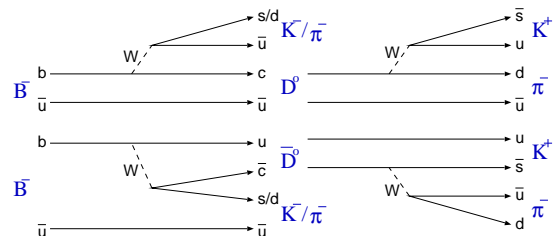


FIG. 1: $B^- \rightarrow [K^+\pi^-]_D K^-$ and $B^- \rightarrow [K^+\pi^-]_D \pi^-$ decays.

decay modes as follows:

$$\begin{aligned} \text{Suppressed decay } & B^- \rightarrow [K^+\pi^-]_D h^- \quad B^- \rightarrow D_{\text{sup}} h^- \\ \text{Favored decay } & B^- \rightarrow [K^-\pi^+]_D h^- \quad B^- \rightarrow D_{\text{fav}} h^- \end{aligned}$$

The results are based on a data sample containing 275 million $B\bar{B}$ pairs, collected with the Belle detector at the KEKB asymmetric energy e^+e^- collider [6] operating at the $\Upsilon(4S)$ resonance. The Belle detector is a large-solid-angle magnetic spectrometer that consists of a silicon vertex detector (SVD), a 50-layer central drift chamber (CDC), an array of aerogel threshold Čerenkov counters (ACC), a barrel-like arrangement of time-of-flight scintillation counters (TOF), and an electromagnetic calorimeter (ECL) comprised of CsI(Tl) crystals located inside a superconducting solenoid coil that provides a 1.5 T magnetic field. An iron flux-return located outside of the

coil is instrumented to detect K_L^0 mesons and to identify muons (KLM). The detector is described in detail elsewhere [7]. Two different inner detector configurations were used. For the first sample of 152 million $B\bar{B}$ pairs, a 2.0 cm radius beampipe and a 3-layer silicon vertex detector were used; for the latter 123 million $B\bar{B}$ pairs, a 1.5 cm radius beampipe, a 4-layer silicon detector and a small-cell inner drift chamber were used [8].

Neutral D mesons are reconstructed by combining two oppositely charged tracks. For each track, information from ACC, TOF and specific ionization measurements from the CDC are used to determine a K/π likelihood ratio $P(K/\pi) = \mathcal{L}_K/(\mathcal{L}_K + \mathcal{L}_\pi)$, where \mathcal{L}_K and \mathcal{L}_π are kaon and pion likelihoods. We use the particle identification requirements $P(K/\pi) > 0.8$ for kaons and $P(K/\pi) < 0.2$ for pions. These requirements select kaons (pions) with momentum dependent efficiencies of 80 – 95% (90 – 95%) and pion (kaon) misidentification probabilities of 5 – 20% (15 – 20%). D candidates are required to have an invariant mass within $\pm 2.5\sigma$ of the nominal D mass: $1.850 \text{ GeV}/c^2 < M(K\pi) < 1.879 \text{ GeV}/c^2$. To improve the momentum determination, tracks from the D candidate are refitted according to the nominal D mass hypothesis and the reconstructed vertex position (a mass-and-vertex-constrained fit). B mesons are reconstructed by combining D candidates with primary charged hadron candidates. The signal is identified by two kinematic variables, the energy difference $\Delta E = E_D + E_{h^-} - E_{\text{beam}}$ and the beam-energy-constrained mass $M_{\text{bc}} = \sqrt{E_{\text{beam}}^2 - (\vec{p}_D + \vec{p}_{h^-})^2}$, where E_D is the energy of the D candidate, E_{h^-} is the energy of the h^- , and E_{beam} is the beam energy, all evaluated in the center-of-mass (cm) frame; \vec{p}_D and \vec{p}_{h^-} are the momenta of the D and h^- in the cm frame. Event candidates are accepted if they have $5.2 \text{ GeV}/c^2 < M_{\text{bc}} < 5.3 \text{ GeV}/c^2$ and $|\Delta E| < 0.2 \text{ GeV}$. If there is more than one candidate in an event, we select the best candidate on the basis of a χ^2 determined from the difference between the measured and nominal values of $M(K\pi)$ and M_{bc} .

To suppress the large background from the two-jet-like $e^+e^- \rightarrow q\bar{q}$ ($q = u, d, s, c$) continuum processes, variables that characterize the event topology are used. We construct a Fisher discriminant [9] of Fox-Wolfram moments called the Super-Fox-Wolfram (*SFW*) [10], where the Fisher coefficients are optimized by maximizing the separation between $B\bar{B}$ events and continuum events. Furthermore, $\cos\theta_B$, the cosine of the angle in the cm system between the B flight direction with respect to the beam axis is also used to distinguish $B\bar{B}$ events from continuum events. These two independent variables, *SFW* and $\cos\theta_B$, are combined to form a likelihood ratio $\mathcal{R} = \mathcal{L}_{\text{sig}}/(\mathcal{L}_{\text{sig}} + \mathcal{L}_{\text{cont}})$, where \mathcal{L}_{sig} and $\mathcal{L}_{\text{cont}}$ are likelihoods calculated from the *SFW* and $\cos\theta_B$ distributions of signal and continuum background events, respectively. We optimize the \mathcal{R} requirement by maximizing $S/\sqrt{S+N}$, where S and N denote the expected

numbers of signal and background events in the signal region. For $B^- \rightarrow D_{\text{sup}}K^-$ ($B^- \rightarrow D_{\text{sup}}\pi^-$) we require $\mathcal{R} > 0.85$ ($\mathcal{R} > 0.75$), which retains 44.8% (57.6%) of the signal events and removes 96.2% (93.2%) of the continuum background.

For $B^- \rightarrow D_{\text{sup}}K^-$, there can be a contribution from $B^- \rightarrow D^0\pi^-$, $D^0 \rightarrow K^+K^-$, which has the same final state and can peak under the signal. In order to reject these events, we veto events that satisfy $1.843 \text{ GeV}/c^2 < M(KK) < 1.894 \text{ GeV}/c^2$. The favored decay $B^- \rightarrow D_{\text{fav}}h^-$ can also cause a peaking background for the suppressed decay modes if both the kaon and pion from the D_{fav} decay are misidentified. Therefore, we veto events for which the invariant mass of the $K\pi$ pair is inside the D mass window when the mass assignments are exchanged. After applying this veto, the residual background from $K\pi$ misidentification is found to be negligible. The three-body charmless decay $B^- \rightarrow K^+K^-\pi^-$ can peak inside the signal regions of ΔE and M_{bc} for $B^- \rightarrow D_{\text{sup}}K^-$. This background is estimated from the ΔE distribution of events in a D mass sideband, defined as $1.637 \text{ GeV}/c^2 < M(K\pi) < 1.836 \text{ GeV}/c^2$ and $1.893 \text{ GeV}/c^2 < M(K\pi) < 2.093 \text{ GeV}/c^2$. The estimated peaking background inside the ΔE signal region is 1.7 ± 0.9 events, which we subtract from the observed $B^- \rightarrow D_{\text{sup}}K^-$ yield. As a check, we estimate the expected background level from the measured $B^- \rightarrow K^+K^-\pi^-$ branching fraction [11]. Using this result, the expected background in our signal region is 2.1 ± 0.6 events, assuming that the $B^- \rightarrow K^+K^-\pi^-$ yield is uniformly distributed in phase space. For $B^- \rightarrow D_{\text{sup}}\pi^-$, the peaking background estimated from the D mass sideband is consistent with zero.

The signal yields are extracted using binned maximum likelihood fits to the ΔE distributions of events in the M_{bc} signal region, ($5.27 \text{ GeV}/c^2 < M_{\text{bc}} < 5.29 \text{ GeV}/c^2$). Backgrounds from decays such as $B^- \rightarrow D\rho^-$ and $B^- \rightarrow D^*\pi^-$ are distributed in the negative ΔE region and make a small contribution to the signal region. The shape of this $B\bar{B}$ background is modeled with a smoothed histogram obtained from generic Monte Carlo (MC) samples. The continuum background populates the entire ΔE region. The shape of the continuum background is modeled with a linear function. The slope is determined from the ΔE distribution of the M_{bc} sideband ($5.20 \text{ GeV}/c^2 < M_{\text{bc}} < 5.26 \text{ GeV}/c^2$). The ΔE fitting function is the sum of two Gaussians for the signal, the linear function for the continuum, and the smoothed histogram for the $B\bar{B}$ background distribution.

In the fit to the ΔE distribution of $B^- \rightarrow D_{\text{fav}}\pi^-$, the free parameters are the position, width and area of the signal peak, and the normalizations of continuum and $B\bar{B}$ backgrounds. For the signal, the relative widths and areas of the two Gaussians are fixed from the signal MC. For the $B^- \rightarrow D_{\text{fav}}K^-$ fit, the position and width of the signal peak are fixed from the $B^- \rightarrow D_{\text{fav}}\pi^-$ fit results.

TABLE I: Summary of the results. For the $B^- \rightarrow D_{\text{sup}}K^-$ signal yield, the peaking background contribution has been subtracted. The first two errors on the measured production branching fractions are statistical and systematic, respectively, and the third is due to the uncertainty in the $B^- \rightarrow D_{\text{fav}}h^-$ product branching fraction used for normalization.

Mode	Product branching fraction from [12]	Efficiency (%)	Signal Yield	Statistical significance	Measured product branching fraction	Upper limit (90%C.L.)
$B^- \rightarrow D_{\text{sup}}K^-$	—	12.9 ± 0.2	$8.5^{+6.0}_{-5.3}$	2.3σ	$(3.2^{+2.2}_{-2.0} \pm 0.2 \pm 0.5) \times 10^{-7}$	6.3×10^{-7}
$B^- \rightarrow D_{\text{sup}}\pi^-$	$(6.9 \pm 0.7) \times 10^{-7}$	20.1 ± 0.2	$28.5^{+8.1}_{-7.4}$	6.4σ	$(6.6^{+1.9}_{-1.7} \pm 0.4 \pm 0.3) \times 10^{-7}$	—
$B^- \rightarrow D_{\text{fav}}K^-$	$(1.4 \pm 0.2) \times 10^{-5}$	12.9 ± 0.2	$376.0^{+21.8}_{-21.1}$	—	—	—
$B^- \rightarrow D_{\text{fav}}\pi^-$	$(1.9 \pm 0.1) \times 10^{-4}$	20.3 ± 0.2	$8181.9^{+94.0}_{-93.3}$	—	—	—

To fit the feed-across from $B^- \rightarrow D_{\text{fav}}\pi^-$, we use a Gaussian shape where the left and right sides of the peak have different widths since the shift caused by wrong mass assignment makes the shape asymmetric. The shape parameters of this function are fixed to values determined by the fit to the $B^- \rightarrow D_{\text{fav}}\pi^-$ distribution using a kaon mass hypothesis for the prompt pion. The areas of signal and feed-across from $B^- \rightarrow D\pi^-$, and the normalizations of continuum and $B\bar{B}$ backgrounds are floated in the fit. For $B^- \rightarrow D_{\text{sup}}K^-$ and $B^- \rightarrow D_{\text{sup}}\pi^-$, the signal and $B\bar{B}$ background shapes are modeled using the fit results for the $B^- \rightarrow D_{\text{fav}}K^-$ and $B^- \rightarrow D_{\text{fav}}\pi^-$ modes, respectively. The area of the feed-across from $D_{\text{sup}}\pi^-$ is estimated as the measured yield of $B^- \rightarrow D_{\text{sup}}\pi^-$ multiplied by the π to K misidentification probability. However, the areas of the signal and the normalizations of continuum and $B\bar{B}$ backgrounds are floated. The fit results are shown in Fig. 2. The numbers of events for $B^- \rightarrow D_{\text{sup}}h^-$ and $D_{\text{fav}}h^-$, and the statistical significances of the $B^- \rightarrow D_{\text{sup}}h^-$ signals are given in Table I. The statistical significance is defined as $\sqrt{-2 \ln(\mathcal{L}_0/\mathcal{L}_{\text{max}})}$, where \mathcal{L}_{max} is the maximum likelihood in the ΔE fit and \mathcal{L}_0 is the likelihood when the signal yield is constrained to be zero. The uncertainty in the peaking background contribution is taken into account in the statistical significance calculation.

The ratio of branching fractions is defined as

$$R_{Dh} \equiv \frac{\mathcal{B}(B^- \rightarrow D_{\text{sup}}h^-)}{\mathcal{B}(B^- \rightarrow D_{\text{fav}}h^-)} = \frac{N_{D_{\text{sup}}h^-}/\epsilon_{D_{\text{sup}}h^-}}{N_{D_{\text{fav}}h^-}/\epsilon_{D_{\text{fav}}h^-}},$$

where $N_{D_{\text{sup}}h}$ ($N_{D_{\text{fav}}h}$) and $\epsilon_{D_{\text{sup}}h^-}$ ($\epsilon_{D_{\text{fav}}h^-}$) are the number of signal events and the reconstruction efficiency for the decay $B^- \rightarrow D_{\text{sup}}h^-$ ($B^- \rightarrow D_{\text{fav}}h^-$), and are given in Table I.

The ratios R_{Dh} are calculated to be

$$R_{DK} = (2.3^{+1.6}_{-1.4}(\text{stat}) \pm 0.1(\text{syst})) \times 10^{-2},$$

$$R_{D\pi} = (3.5^{+1.0}_{-0.9}(\text{stat}) \pm 0.2(\text{syst})) \times 10^{-3}.$$

Since the signal for $B^- \rightarrow D_{\text{sup}}K^-$ is not significant, we set an upper limit at the 90% confidence level (C.L.) of $R_{DK} < 4.4 \times 10^{-2}$, where we take the likelihood function as a single Gaussian with width given by the quadratic sum of statistical and systematic errors, and the area is

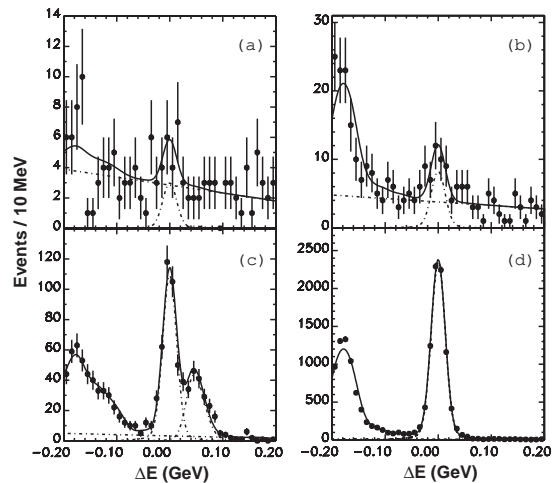


FIG. 2: ΔE fit results for (a) $B^- \rightarrow D_{\text{sup}}K^-$, (b) $B^- \rightarrow D_{\text{sup}}\pi^-$, (c) $B^- \rightarrow D_{\text{fav}}K^-$, and (d) $B^- \rightarrow D_{\text{fav}}\pi^-$. Charge conjugate modes are included in these plots.

normalized in the physical region of positive branching fraction.

Most of the systematic uncertainties from the detection efficiencies and the particle identification cancel when taking the ratios, since the kinematics of the $B^- \rightarrow D_{\text{sup}}h^-$ and $B^- \rightarrow D_{\text{fav}}h^-$ processes are similar. The systematic errors are due to uncertainties in the yield extraction (4.7%–5.4%) and the efficiency difference between $B^- \rightarrow D_{\text{sup}}h^-$ and $B^- \rightarrow D_{\text{fav}}h^-$ (1.3%–1.7%). The uncertainties in the signal shapes and the $q\bar{q}$ background shapes are determined by varying the shape of the fitting function by $\pm 1\sigma$. The uncertainties in the $B\bar{B}$ background shapes are determined by fitting the ΔE distribution in the region $-0.07 \text{ GeV} < \Delta E < 0.20 \text{ GeV}$ ignoring the $B\bar{B}$ background contributions. The uncertainties in the efficiency differences are determined using signal MC. The total systematic error is the sum in quadrature of the above uncertainties.

The product branching fractions for $B^- \rightarrow D_{\text{sup}}h^-$ are determined as

$$\mathcal{B}(B^- \rightarrow D_{\text{sup}}h^-) = \mathcal{B}(B^- \rightarrow D_{\text{fav}}h^-) \times R_{Dh},$$

and are given in Table I. A third uncertainty arises due

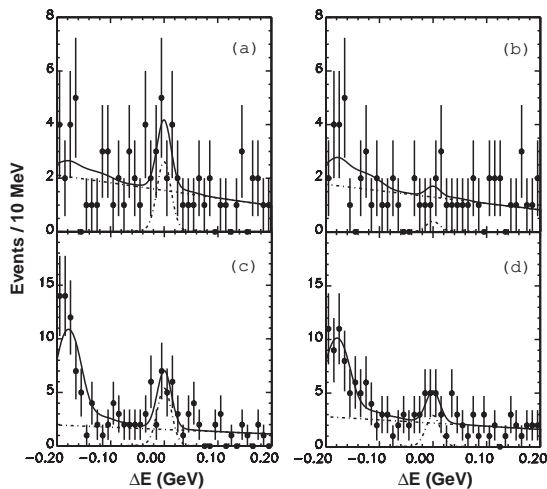


FIG. 3: ΔE fit results for (a) $B^- \rightarrow D_{\text{sup}}K^-$, (b) $B^+ \rightarrow D_{\text{sup}}K^+$, (c) $B^- \rightarrow D_{\text{sup}}\pi^-$, and (d) $B^+ \rightarrow D_{\text{sup}}\pi^+$.

TABLE II: Signal yields and partial rate asymmetries.

Mode	$N(B^-)$	$N(B^+)$	\mathcal{A}_{Dh}
$B \rightarrow D_{\text{sup}}K$	$8.2^{+5.0}_{-4.3}$	$0.5^{+3.5}_{-2.8}$	$0.88^{+0.77}_{-0.62} \pm 0.06$
$B \rightarrow D_{\text{sup}}\pi$	$18.8^{+6.3}_{-5.5}$	$10.1^{+5.5}_{-4.8}$	$0.30^{+0.29}_{-0.25} \pm 0.06$

to the error in the branching fraction of $B^- \rightarrow D_{\text{fav}}h^-$, which is taken from [12]. The uncertainties are statistics-dominated. For the $B^- \rightarrow D_{\text{sup}}K^-$ branching fraction, we set an upper limit at the 90% C.L. of $\mathcal{B}(B^- \rightarrow D_{\text{sup}}K^-) < 6.3 \times 10^{-7}$. For $B^- \rightarrow D_{\text{sup}}\pi^-$, our measured branching fraction is consistent with expectation neglecting the contribution from $B^- \rightarrow \bar{D}^0\pi^-$.

The ratio R_{DK} is related to ϕ_3 by

$$R_{DK} = r_B^2 + r_D^2 + 2r_B r_D \cos \phi_3 \cos \delta,$$

where [12]

$$r_B \equiv \left| \frac{A(B^- \rightarrow \bar{D}^0 K^-)}{A(B^- \rightarrow D^0 K^-)} \right|, \quad \delta \equiv \delta_B + \delta_D,$$

$$r_D \equiv \left| \frac{A(D^0 \rightarrow K^+ \pi^-)}{A(D^0 \rightarrow K^- \pi^+)} \right| = 0.060 \pm 0.003,$$

and δ_B and δ_D are the strong phase differences between the two B and D decay amplitudes, respectively. Using the above result, we obtain a limit on r_B . The least restrictive limit is obtained allowing $\pm 1\sigma$ variation on r_D and assuming maximal interference ($\phi_3 = 0^\circ, \delta = 180^\circ$ or $\phi_3 = 180^\circ, \delta = 0^\circ$) and is found to be $r_B < 0.27$.

We search for partial rate asymmetries \mathcal{A}_{Dh} in $B^\mp \rightarrow D_{\text{sup}}h^\mp$ decay, fitting the B^- and B^+ yields separately for each mode, where \mathcal{A}_{Dh} is determined as

$$\mathcal{A}_{Dh} \equiv \frac{\mathcal{B}(B^- \rightarrow D_{\text{sup}}h^-) - \mathcal{B}(B^+ \rightarrow D_{\text{sup}}h^+)}{\mathcal{B}(B^- \rightarrow D_{\text{sup}}h^-) + \mathcal{B}(B^+ \rightarrow D_{\text{sup}}h^+)}.$$

The peaking background for $B^\mp \rightarrow D_{\text{sup}}K^\mp$ is subtracted assuming no CP asymmetry. The fit results are shown in Fig. 3 and Table II. We find

$$\mathcal{A}_{DK} = 0.88^{+0.77}_{-0.62}(\text{stat}) \pm 0.06(\text{syst}),$$

$$\mathcal{A}_{D\pi} = 0.30^{+0.29}_{-0.25}(\text{stat}) \pm 0.06(\text{syst}),$$

where the systematic uncertainties arise from possible biases in the analysis algorithms (estimated from the $B^\mp \rightarrow D_{\text{fav}}\pi^\mp$ control sample to be 2.5%); uncertainties in the extraction of the B^- and B^+ yields (estimated by varying fitting parameters by $\pm 1\sigma$ to be 4.9%); asymmetry in the particle identification efficiency of prompt kaons (estimated in [13] to be 0.6%). We assume no CP asymmetry in the peaking background, and do not assign any systematic uncertainty from this source [14].

In summary, using 275 million $B\bar{B}$ pairs collected with the Belle detector, we report studies of the suppressed decay $B^- \rightarrow D_{\text{sup}}h^-$ ($h = K, \pi$). We observe $B^- \rightarrow D_{\text{sup}}\pi^-$ for the first time, with a significance of 6.4 σ . The size of the signal is consistent with expectation based on measured branching fractions [12]. The significance for $B^- \rightarrow D_{\text{sup}}K^-$ is 2.3 σ and we set an upper limit on the ratio of B decay amplitudes $r_B < 0.27$ at 90% confidence level. This result is consistent with previous searches [5], and with the measurement of r_B in the decay $B^- \rightarrow DK^-$, $D \rightarrow K_S^0\pi^+\pi^-$ [15], which provides the most precise current determination of ϕ_3 .

We thank the KEKB group for the excellent operation of the accelerator, the KEK Cryogenics group for the efficient operation of the solenoid, and the KEK computer group and the NII for valuable computing and SuperSINET network support. We acknowledge support from MEXT and JSPS (Japan); ARC and DEST (Australia); NSFC (contract No. 10175071, China); DST (India); the BK21 program of MOEHRD and the CHEP SRC program of KOSEF (Korea); KBN (contract No. 2P03B 01324, Poland); MIST (Russia); MESS (Slovenia); NSC and MOE (Taiwan); and DOE (USA).

* on leave from Nova Gorica Polytechnic, Nova Gorica

- [1] M. Kobayashi and T. Maskawa, Prog. Theor. Phys. **49**, 652 (1973).
- [2] I.I. Bigi and A.I. Sanda, Phys. Lett. B **211**, 213 (1988).
- [3] M. Gronau and D. Wyler, Phys. Lett. B **165**, 172 (1991); M. Gronau and D. London, Phys. Lett. B **253**, 483 (1991).
- [4] D. Atwood, I. Dunietz, and A. Soni, Phys. Rev. Lett. **78**, 3257 (1997), Phys. Rev. D **63**, 036005 (2001).
- [5] B. Aubert *et al.* (BaBar collaboration), Phys. Rev. Lett. **93**, 131804 (2004).
- [6] S. Kurokawa and E. Kikutani, Nucl. Instr. and Meth. A **499**, 1 (2003).
- [7] A. Abashian *et al.* (Belle collaboration), Nucl. Instr. and Meth. A **479**, 117 (2002).

- [8] Y. Ushiroda (Belle SVD2 Group), Nucl. Instr. and Meth. A **511**, 6 (2003).
- [9] R.A. Fisher, Ann. Eugenics **7**, 179 (1936).
- [10] The Fox-Wolfram moments were introduced in G.C. Fox and S. Wolfram, Phys. Rev. Lett. **41**, 1581 (1978). The Fisher discriminant used by Belle, based on modified Fox-Wolfram moments (SFW), is described in K. Abe *et al.* (Belle collaboration), Phys. Rev. Lett. **87**, 101801 (2001).
- [11] A. Garmash *et al.* (Belle collaboration), Phys. Rev. D **69**, 012001 (2004).
- [12] S. Eidelman *et al.* (Particle Data Group), Phys. Lett. B **592**, 1 (2004).
- [13] Y. Chao *et al.* (Belle collaboration), Phys. Rev. Lett. **93**, 191802 (2004).
- [14] An assumption of 30% CP asymmetry in the peaking background would lead to a shift of 5.5% in \mathcal{A}_{DK} .
- [15] A. Poluektov *et al.* (Belle collaboration), Phys. Rev. D **70**, 072003 (2004).